applied optics

Giant circular dichroism induced by silver nanocuboid heterodimers

WAN ZHANG, YONGKAI WANG, XIAOJING WEN, AND ZHONGYUE ZHANG*

School of Physics and Information Technology, Shaanxi Normal University, Xi'an 710062, China
**Corresponding author: zyzhang@snnu.edu.cn*

Received 30 July 2015; revised 20 September 2015; accepted 30 September 2015; posted 9 October 2015 (Doc. ID 246799); published 30 October 2015

Metallic nanocuboid heterodimers are proposed to generate a giant circular dichroism (CD) effect. Two cuboids in the heterodimers have different heights. The dipole and quadrupole charge oscillation modes in the cuboids occur under left- and right-handed circular polarizations. The height difference generates phase difference between charge oscillations in the two cuboids. The two charge oscillations and the phase difference between them are consistent with the Born–Kuhn model for the CD effect. The CD effect of the nanocuboid heterodimers can be tuned by changing the structural parameters of the nanocuboid heterodimers, especially the height difference between two cuboids. The results of this research are not only useful for designing plasmonic structures to generate the CD effect but also for understanding the physical mechanisms of the CD effect.

OCIS codes: (100.1930) Dichroism; (160.1585) Chiral media; (250.5403) Plasmonics.

http://dx.doi.org/10.1364/AO.54.009359

1. INTRODUCTION

Circular dichroism (CD) is the different optical response induced by lights that are left-handed circularly polarized (LCP) and right-handed circularly polarized (RCP) photons [1]. CD is commonly observed in chiral structures that lack mirror-image symmetry [2–5]. Chiral structures with CD are always related to circular polarizers for optoelectronic conversion [6,7], polarization conversion [8,9], and molecular analysis [10–13].

Numerous investigations primarily considered achiral single-layer metal structures that exhibit CD effects under oblique illumination [14–16]. When nanorice heterodimers are placed under illumination at oblique angles, electric dipoles in large nanorice are not parallel to electric dipoles in small nanorice. A phase difference exists between them, and this difference generates chiral optical activity [15]. 3D chiral structures, including various metallic helix materials [17,18] and layer-by-layer chiral metal structures [19–21], generate giant chirality responses. When Ag nanohelixes are illuminated by LCP and RCP incidences, different collective charge oscillations of effective dipole length appear within a half-pitch along the helix [18]. The coupling between dipoles within adjacent pitches leads to CD effects. In the chiral plasmonic structure of two identical corner-stacked and vertically displaced nanorods with a twist angle, phase retardation effects lead to different charge oscillation modes under LCP and RCP incidences, which can also generate a CD effect [21]. The simplest version of the Born–Kuhn configuration provides the fundamental optical chiral activity explanation with bonding and antibonding modes [21,22]. The Born–Kuhn configuration explains the CD mechanism of various structures including helix, layer-by-layer, and achiral structures under oblique illumination [23–28].

In this study chiral nanocuboid heterodimers consisting of two silver cuboids with different sizes were designed to generate a CD effect. The results show that the nanocuboid heterodimers can produce a giant CD effect, and the CD signal can be tuned by varying the structural parameters. The CD mechanism in the nanocuboid heterodimers satisfies the Born–Kuhn model. The dipole and quadruple charge oscillations in the two cuboids form the bonding and antibonding modes, and the height difference generates a phase difference between charge oscillations. This study not only presents a simple method to produce nanostructures to generate a CD effect but also helps in the understanding of the mechanism of CD effects.

2. STRUCTURE AND COMPUTATIONAL METHOD

The configuration of Ag nanocuboid heterodimer arrays and their structural parameters are illustrated in Fig. 1. The nanocuboid heterodimers consist of a large silver cuboid with length L, width W, and height H, and a small silver cuboid with fixed length $l = 100$ nm, width $w = 50$ nm, and height $h = 50$ nm. As shown in Fig. 1 the two cuboids share the x–y plane at the bottom and the y–z plane at their ends. In addition the

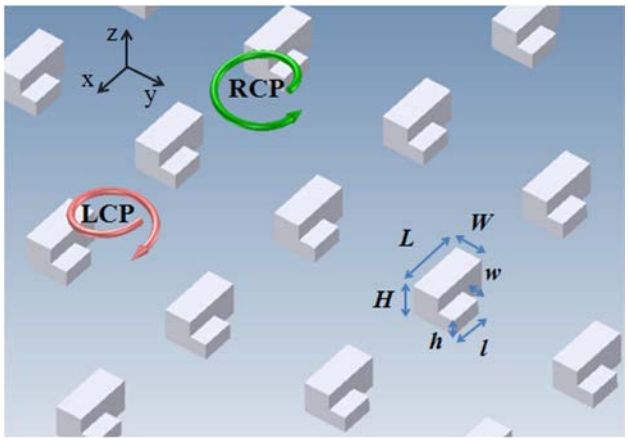

Fig. 1. Schematics of the configuration of the silver nanocuboid heterodimer arrays.

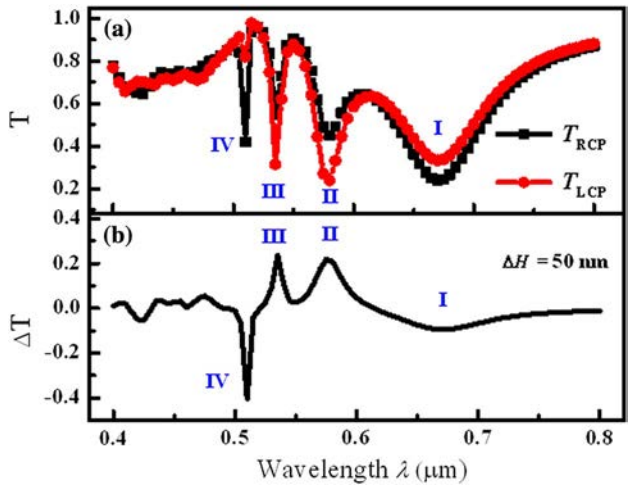

Fig. 2. (a) Simulated transmission spectra of LCP and RCP light for the chiral heterodimers. (b) Differences of transmittance spectra of heterodimers with $\Delta H = 50$ nm between LCP light and RCP light.

two cuboids are parallel and cling to each other. The unit cell has a dimension of 500 nm × 500 nm on the x–y plane.

The frequency-dependent permittivity values of Ag were derived from [29]. The transmission properties were simulated with the 3D commercial finite-element method software COMSOL Multiphysics. Circularly polarized light (left- and right-handed) was illuminated normally to the nanocuboid heterodimer arrays. Transmittance was defined as $T = P_{out}/P_{in}$, which is the ratio of output power to incident power. T_{RCP} is defined as RCP to RCP transmittance, which is the ratio of the output power with RCP to the incident power with RCP. T_{LCP} is defined as LCP to LCP transmittance, which is the ratio of the output power with LCP to the incident power with LCP. The CD effect was defined as $\Delta T = T_{RCP} - T_{LCP}$.

3. RESULTS AND DISCUSSION

Figure 2(a) shows the transmission spectra of the nanocuboid heterodimer arrays under RCP and LCP light illuminations. The structural parameters of the large nanocuboids are $L = 180$ nm, $W = 80$ nm, and $H = 100$ nm. Thus, the height difference between the two cuboids is $\Delta H = H - h = 50$ nm. Four resonant modes, namely, $\lambda_I = 0.670$ μm, $\lambda_{II} = 0.580$ μm, $\lambda_{III} = 0.535$ μm, and $\lambda_{IV} = 0.510$ μm appear in the transmission spectra under both RCP and LCP illuminations. Figure 2(b) shows the CD effect of the nanocuboid heterodimer arrays. Four CD peaks or valleys appear at the resonant wavelengths. At modes I and IV, transmittances under LCP illumination are larger than those under RCP illumination. At modes II and III, transmittances under RCP illumination are larger than those under LCP illumination.

In addition, the conversions of this heterodimer were also calculated. Larger conversions occur at resonant wavelength with a density less than 20%.

To investigate the transmission mechanism of the nanocuboid heterodimers under circular illumination, we examined the distributions of surface current density, the paths of charge oscillations, and the steady-state electric-field distributions of the chiral heterodimers at resonant modes, as depicted in Fig. 3. Figures 3(a1), 3(b1), 3(c1), and 3(d1) show the distributions of surface current density in the heterodimers on the x–y and y–z planes of the four resonant modes. Figures 3(a2), 3(b2), 3(c2), and 3(d2) show the effective charge oscillations in the heterodimers under LCP and RCP illuminations. The eight letters (A–H) denote the corner points of the large cuboid. Solid and dotted lines with arrows illustrate the effective charge oscillation modes. Figures 3(a3), 3(b3), 3(c3), and 3(d3) show the electric fields on the x–y plane with a height equal to that of the small cuboid.

At $\lambda_I = 0.670$ μm under LCP illumination, the main current is along the length of the large cuboid. Strong currents also exist along the width of the small cuboid. Under RCP illumination, the direction currents are contrary to those in Fig. 3(a1). As shown in Fig. 3(a2), under LCP illumination the effective charge oscillation from the center of plane ABCD to the center of plane EFGH can be regarded as a dipole, which is

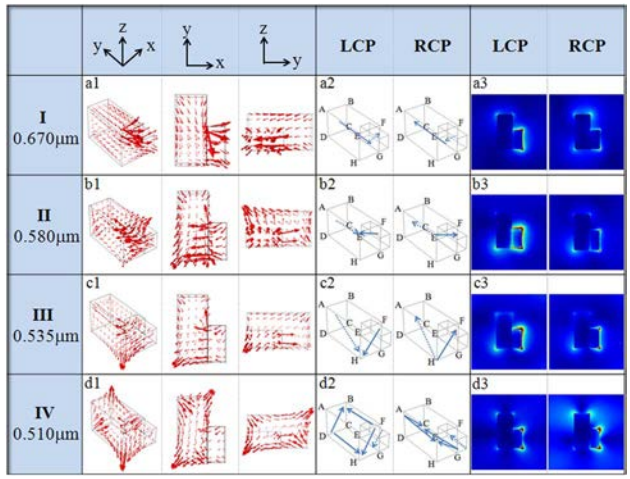

Fig. 3. (a1–d1) Distributions of surface current density of the chiral heterodimers, (a2–d2) detail path of resonant modes, and (a3–d3) steady-state electric field distributions of the chiral heterodimers under the illumination of RCP and LCP.

denoted by the solid line in the heterodimers. The effective charge oscillation perpendicular to the small cuboid can also be regarded as a dipole in the small cuboid, which is denoted by the dotted line in the heterodimers. These two effective dipoles form a bonding mode. The height difference between these two effective dipoles leads to a phase difference between them. Thus, mode I can be regarded as the Born–Kuhn model for the CD effect. Considering that the effective dipole oscillation in the large cuboid is stronger than that in the small cuboid, mode I is mainly determined by the effective dipole mode in the large cuboid. The strong effective dipole oscillation in the large cuboid results in strong electric fields around the corners of the large cuboid as shown in Fig. 3(a3). The strength of electric dipole oscillation under LCP illumination in the large cuboid is less than that under RCP illumination, which results in a negative CD signal of mode I in Fig. 2(b).

At $\lambda_{II} = 0.580$ μm under LCP illumination, the main current is along the width of the small cuboid to a vertex of the large cuboid. Strong currents also exist along the length of the large cuboid. Under RCP illumination the direction currents are contrary to those in Fig. 3(b1). As shown in Fig. 3(b2) under LCP illumination, the effective charge oscillation along the width of the small cuboid to the E vertex can be regarded as a dipole (denoted by a solid line). The effective charge oscillation from the center of plane ABCD to the E vertex can also be regarded as a dipole (denoted by a dotted line). These two effective dipoles form an antibonding mode. Mode II is mainly determined by the effective dipole mode along the small cuboid to the E vertex. The strong effective dipole oscillation also results in strong electric fields around the corners of the small cuboid as shown in Fig. 3(b3). The strength of electric dipole oscillation under RCP illumination in the large cuboid is less than that under LCP illumination, which results in a positive CD signal of mode II in Fig. 2(b).

At $\lambda_{III} = 0.535$ μm, as shown in Fig. 3(c2), under LCP illumination the effective charge oscillation along the width of small cuboid to H vertex can be regarded as a dipole (denoted by a solid line). The effective charge oscillation from the center of plane ABCD to the H vertex can also be regarded as a dipole (denoted by a dotted line). These two effective dipoles form an antibonding mode. Mode III is mainly determined by the effective dipole mode along the small cuboid to the H vertex. The strength of electric dipole oscillation under RCP illumination in the large cuboid is less than that under LCP illumination, which results in a positive CD signal of mode III in Fig. 2(b).

At $\lambda_{IV} = 0.510$ μm, as shown in Fig. 3(d2), under LCP illumination the effective charge oscillation along the D and F vertexes to the B and H vertexes of large cuboid can be regarded as a quadruple (denoted by a solid line). The effective charge oscillation in small cuboid can also be regarded as a dipole (denoted by a dotted line). The two quadruple and dipole form a bonding mode. Mode IV is mainly determined by the effective quadruple mode in the large cuboid. The strength of electric dipole oscillation under LCP illumination in the large cuboid is less than that under RCP illumination, which results in a negative CD signal of mode IV in Fig. 2(b).

The chiral system of the nanocuboid heterodimer can be viewed as a right-handed enantiomer [21,22] in which bonding modes (modes I and IV) are easier to be excited under RCP illumination than under LCP illumination. Conversely, antibonding modes (modes II and mode III) are easier to be excited under LCP illumination than under RCP illumination.

The height difference between the two cuboids leads to a phase difference between effective charge oscillations in the two cuboids, which are the main part of the mechanism of the CD effect. To investigate the height difference in the CD effect of heterodimers, the height of the large cuboid was varied between 50 and 130 nm.

Figure 4 presents the simulated CD effect of heterodimers with $H = 50$, 70, 90, 110, and 130 nm at fixed $L = 180$ nm and $W = 80$ nm. Thus, height difference $\Delta H = 0$, 20, 40, 60, and 80 nm. Since the CD is due to strong near-field coupling and intricate phase retardation effects originated from height difference, the CD effect disappears when the height difference is equal to zero. For $\Delta H = 0$ nm, the CD effect does not exist. The CD effect becomes increasingly obvious as ΔH increases. With the increase in ΔH, the aspect ratio of charge oscillations in the large cuboid decreases, leading to a slight blue-shift of λ_I. Given that mode II is due to the effective dipole oscillation from the small cuboid to the corner of E, the increase in ΔH would increase the oscillation length and result in a red-shift of mode II. Similarly, mode III red-shifts with increased ΔH. The increase in ΔH would increase the charge oscillation length in the quadrupole mode and lead to the red shift of mode IV.

Figure 5 shows the simulated CD effect of heterodimers with $L = 160$, 170, 180, 190, and 200 nm at a fixed $H = 100$ nm and $W = 80$ nm. With the increase in L, the aspect ratio of charge oscillations in the large cuboid increases and thus leads to a slight red shift of λ_I. Mode II is due to the effective dipole oscillation from the small cuboid to the corner of E regardless of the length of the large cuboid, which is insensitive to L. Similarly, mode III does not shift as L increases. The wavelength of mode IV is insensitive to L as indicated in Fig. 5.

Figure 6 shows the simulated CD effect of heterodimers with $W = 60$, 70, 80, 90, and 100 nm at a fixed $H = 100$ nm and $L = 180$ nm. With the increase in W, the aspect

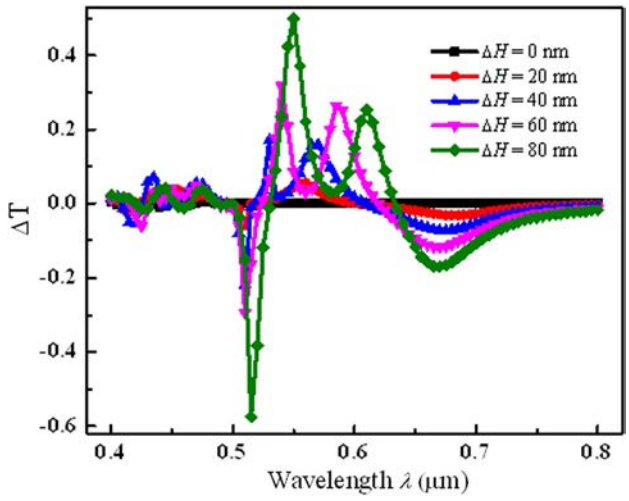

Fig. 4. Simulated differences of transmittance spectra of the chiral heterodimers with different ΔH values.

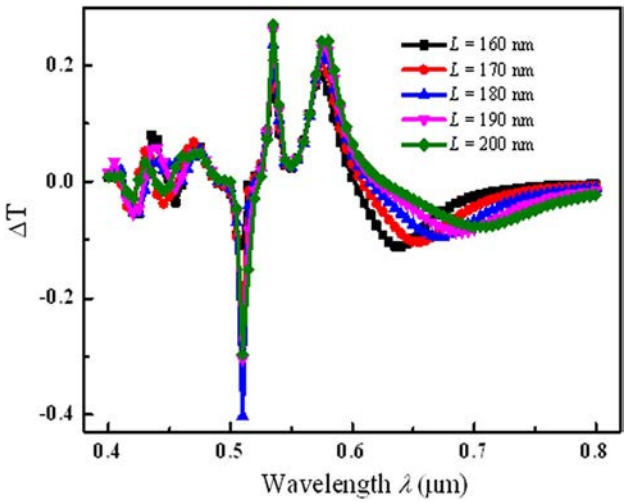

Fig. 5. Simulated differences of transmittance spectra of the chiral heterodimers with different L values.

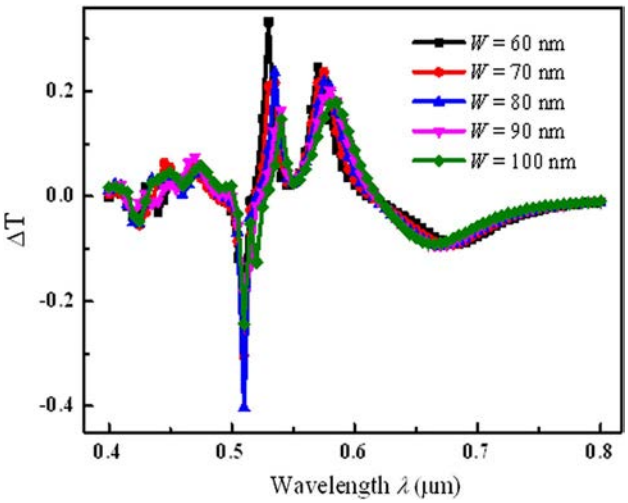

Fig. 6. Simulated differences of transmittance spectra of the chiral heterodimers with different W values.

ratio of charge oscillations in the large cuboid decreases and leads to a slight blue shift of λ_1. Given that mode II is due to the effective dipole oscillation from the small cuboid to the corner of E, the increase in W would increase the oscillation length and result in a red shift of mode II. Similarly, mode III red shifts as W increases. The wavelength of mode IV is insensitive to W as indicated in Fig. 6.

In addition, we also tuned the height, the length, and the width of small cuboid to study the structural effects on the CD effect. Since mode I, mode II, and mode III are associated with the electron oscillations in the small cuboid, they are sensitive to the parameter changes of small cuboid.

4. CONCLUSIONS

Chiral nanocuboid heterodimers were designed, and their CD properties were investigated according to the basic physical mechanism of the CD effect. Transmission spectra, normalized electric-field distribution, and surface current density were investigated through the finite element method software COMSOL Multiphysics. Effective charge oscillations occurred in the heterodimers, and a phase difference was observed between them. The CD mechanism of the nanocuboid heterodimers satisfies the Born–Kuhn model for CD effects. The CD effects of the nanocuboid heterodimers were found to be dependent strongly on structural parameters, especially on the height difference between two cuboids. This investigation can help not only in the design of chiral plasmonic structures to generate CD effects but also in understanding the physical mechanisms of CD effects.

Funding. Fundamental Research Funds for the Central Universities (GK201303007); National Natural Science Foundation of China (NSFC) (11004160).

REFERENCES

1. A. Kuzyk, R. Schreiber, Z. Fan, G. Pardatscher, E.-M. Roller, A. Hogele, C. Simmel, A. O. Govorov, and T. Liedl, "DNA-based self-assembly of chiral plasmonic nanostructures with tailored optical response," Nature **483**, 311–314 (2012).
2. A. O. Govorov, Y. K. Gun'ko, J. M. Slocik, V. A. Gerard, Z. Y. Fan, and R. R. Naik, "Chiral nanoparticle assemblies: circular dichroism, plasmonic interactions, and exciton effects," J. Mater. Chem. **21**, 16806–16818 (2011).
3. B. Yeom, H. N. Zhang, H. Zhang, J. I. Park, K. Kim, A. O. Govorov, and N. A. Kotov, "Chiral plasmonic nanostructures on achiral nanopillars," Nano Lett. **13**, 5277–5283 (2013).
4. X. Wang, W. S. Gao, J. Hung, and W. Y. Tam, "Optical activities of large-area SU8 microspirals fabricated by multibeam holographic lithography," Appl. Opt. **53**, 2425–2430 (2014).
5. V. K. Valev, J. J. Baumberg, C. Sibilia, and T. Verbiest, "Chirality and chiroptical effects in plasmonic nanostructures: fundamentals, recent progress, and outlook," Adv. Mater. **25**, 2517–2534 (2013).
6. Z. Y. Yang, M. Zhao, and P. X. Lu, "A numerical study on helix nanowire metamaterials as optical circular polarizers in the visible region," IEEE Photon. Technol. Lett. **22**, 1303–1305 (2010).
7. S. X. Li, Z. Y. Yang, J. Wang, and M. Zhao, "Broadband terahertz circular polarizers with single- and double-helical array metamaterials," J. Opt. Soc. Am. A **28**, 19–23 (2011).
8. Y. Yu, Z. Y. Yang, S. X. Li, and M. Zhao, "Higher extinction ratio circular polarizers with hetero-structured double-helical metamaterials," Opt. Express **19**, 10886–10894 (2011).
9. J. K. Gansel, M. Latzel, A. Frolich, J. Kaschke, M. Thiel, and M. Wegener, "Tapered gold-helix metamaterials as improved circular polarizers," Appl. Phys. Lett. **100**, 101109 (2012).
10. E. Hendry, R. V. Mikhaylovskiy, L. D. Barron, M. Kadodwala, and T. J. Davis, "Chiral electromagnetic fields generated by arrays of nanoslits," Nano Lett. **12**, 3640–3644 (2012).
11. M. Schaferling, D. Dregely, M. Hentschel, and H. Giessen, "Tailoring enhanced optical chirality: Design principles for chiral plasmonic nanostructures," Phys. Rev. X **2**, 031010 (2012).
12. A. O. Govorov, Z. Y. Fan, P. Hernandez, J. M. Slocik, and R. R. Naik, "Theory of circular dichroism of nanomaterials comprising chiral molecules and nanocrystals: Plasmon enhancement, dipole interactions, and dielectric effects," Nano Lett. **10**, 1374–1382 (2010).
13. R. Ogier, Y. R. Fang, M. Svedendahl, P. Johansson, and M. Kall, "Macroscopic layers of chiral plasmonic nanoparticle oligomers from colloidal lithography," ACS Photonics **1**, 1074–1081 (2014).
14. E. Plum, X. X. Liu, V. A. Fedotov, Y. Chen, D. P. Tsai, and N. I. Zheludev, "Metamaterials:optical activity without chirality," Phys. Rev. Lett. **102**, 113902 (2009).

15. X. R. Tian, Y. R. Fang, and B. Zhang, "Multipolar Fano resonances and Fano-assisted optical activity in silver nanorice heterodimers," ACS Photonics **1**, 1156–1164 (2014).
16. T. Cao, C. W. Wei, and L. Zhang, "Modeling of multi-band circular dichroism using metal/dielectric/metal achiral metamaterials," Opt. Mater. Express **4**, 1526–1534 (2014).
17. J. K. Gansel, M. Wegener, S. Burger, and S. Linden, "Gold helix photonic metamaterials: A numerical parameter study," Opt. Express **18**, 1059–1069 (2010).
18. Z. Y. Zhang and Y. P. Zhao, "The visible extinction peaks of ag nano-helixes: A periodic effective dipole model," Appl. Phys. Lett. **98**, 083102 (2011).
19. B. Frank, X. H. Yin, M. Schaferling, J. Zhao, S. M. Hein, P. V. Braun, and H. Giessen, "Large-area 3D chiral plasmonic structures," ACS Nano **7**, 6321–6329 (2013).
20. L. Wu, Z. Y. Yang, Y. Z. Cheng, Z. Q. Lu, P. Zhang, M. Zhao, R. Z. Gong, X. H. Yuan, Y. Zheng, and J. A. Duan, "Electromagnetic manifestation of chirality in layer-by-layer chiral metamaterials," Opt. Express **21**, 5239–5246 (2013).
21. X. H. Yin, M. Schaferling, B. Metzger, and H. Giessen, "Interpreting chiral nanophotonic spectra: The plasmonic Born–Kuhn model," Nano Lett. **13**, 6238–6243 (2013).
22. Y. H. Cui, L. Kang, S. F. Lan, S. Rodrigues, and W. S. Cai, "Giant chiral optical response from a twisted-arc metamaterial," Nano Lett. **14**, 1021–1025 (2014).
23. J. F. Dong, J. F. Zhou, T. Koschny, and C. Soukoulis, "Bi-layer cross chiral structure with strong optical activity and negative refractive index," Opt. Express **17**, 14172–14179 (2009).
24. M. Decker, M. Ruther, C. E. Kriegler, J. Zhou, C. M. Soukoulis, S. Linden, and M. Wegener, "Strong optical activity from twisted-cross photonic metamaterials," Opt. Lett. **34**, 2501–2503 (2009).
25. R. Zhao, L. Zhang, J. Zhou, T. Koschny, and C. M. Soukoulis, "Conjugated gammadion chiral metamaterial with uniaxial optical activity and negative refractive index," Phys. Rev. B **83**, 035105 (2011).
26. M. Decker, R. Zhao, C. M. Soukoulis, S. Linden, and M. Wegener, "Twisted split-ring-resonator photonic metamaterial with huge optical activity," Opt. Lett. **35**, 1593–1595 (2010).
27. Z. F. Li, R. K. Zhao, T. Koschny, M. Kafesaki, K. B. Alici, E. Colak, H. Caglayan, E. Ozbay, and C. M. Soukoulis, "Chiral metamaterials with negative refractive index based on four "U" split ring resonators," Appl. Phys. Lett. **97**, 081901 (2010).
28. Z. F. Li, K. B. Alici, E. Colak, and E. Ozbay, "Complementary chiral metamaterials with giant optical activity and negative refractive index," Appl. Phys. Lett. **98**, 161907 (2011).
29. P. B. Johnson and R. W. Christy, "Optical constants of the noble metals," Phys. Rev. B **6**, 4370–4379 (1972).